15TH IEA HEAT PUMP CONFERENCE
MAY 26–29, 2026 | HOFBURG
VIENNA 2026
DECARBONISATION THROUGH INNOVATION

"Scroll compressor technology development for next generation refrigerants: Experimental and numerical model development"

Yash Shantilal Parmar[a,*], Samuel Yana Motta[b], Haotian Liu[a,c], Eckhard A. Groll[a], Riley B. Barta[a]

[a]Ray W. Herrick Laboratories, Purdue University, 177 S. Russell Street, West Lafayette, 47907-2099, Indiana, United States
[b]Orbia Fluor & Energy Materials, 4990B ICI Road, Hwy. 75, PO Box 30, St. Gabriel, 70776, Louisiana, United States
[c]Mechanical and Aerospace Engineering, Oklahoma State University, 300 Engineering South, Stillwater, 74078, Oklahoma, United States

Abstract

The imperative to mitigate climate change is driving the HVAC&R industry to transition to low-Global Warming Potential (GWP) refrigerants like R-290 and R-454C, as mandated by global protocols such as Kigali Amendment (2016) and F-Gas Regulation (2024). This study presents experimental evaluations and modelling efforts to support the development of high efficiency scroll compressors tailored for these next generation working fluids. Drop-in tests are performed for R-290 and R-454C using a Hydrochlorofluorocarbon (HCFC)-based scroll compressor, along with tests on a commercially available R-290 compressor and an R-410A baseline compressor. The tests demonstrated that R-290 offers high overall isentropic and volumetric efficiency potential. However, the lower volumetric capacity of these alternative refrigerants limits their delivered capacity compared to R-410A. This highlights the need for a comprehensive compressor redesign that goes beyond simple displacement scaling, as the interaction between refrigerant thermophysical properties and compressor geometry is highly coupled and non-linear. To support this, a high-fidelity, physics-based mechanistic scroll compressor model was developed incorporating detailed geometric features, leakage paths, and motor characteristics. The model was validated against R-410A experimental data, achieving mean absolute percentage errors (MAPE) of 2.4 %, 1.18 % and 2.12 % for mass flow rate, power consumption, and overall isentropic efficiency, respectively, and a mean absolute error (MAE) of 1.74 °C for discharge temperature. This developed model serves as an essential tool for further soft optimization studies to isolate loss mechanisms and define the necessary geometric modifications (e.g. scroll height, volume ratio) to maximize performance for R-290 and R-454C. This combined experimental and modeling approach supports the development of high efficiency compressors for next-generation refrigerants.

Keywords: Low-GWP; Scroll compressor; Drop-in testing; Mechanistic model; Optimization

1. Introduction

The escalating global imperative to mitigate climate change has initiated a regulated transformation within the Heating, Ventilation, Air Conditioning, and Refrigeration (HVAC&R) industry. This transformation is driven primarily through the Montreal Protocol (1987) [1] and its subsequent Kigali Amendment (2016) [2], enforcing a structured global phase-down of high-Global Warming Potential (GWP) hydrofluorocarbons (HFCs) [3]. Complementing this international effort, the third iteration of the European Union's F-Gas Regulation (2024) [4] and U.S. AIM act (2020) [5] accelerate the transition by setting stringent sector-based deadlines starting in 2025. This aggressive legislative shift necessitates the industry to rapidly adopt new, alternative working fluids, primarily focusing on natural refrigerants, such as R-290 (propane) [6], and Hydrofluoroolefin (HFO) blends, such as R-454C [7], both of which fall beneath the critical GWP threshold of 150 [8] for R-410A replacements.

* Corresponding author. Tel.: +765-694-9061
E-mail address: parmary@purdue.edu

While R-290 and R-454C are promising from an environmental standpoint, their thermophysical properties differ substantially from R-410A, resulting in significant implications for compressor performance and design. For example, R-290 exhibits a notably lower inlet density coupled with a higher latent heat of vaporization compared to baseline R-410A as shown in Table 1. In contrast, R-454C presents both a lower inlet density and a reduced latent heat compared to R-410A [9-11]. In addition, R-290 is classified as A3 (highly flammable) and R-454C as A2L (mildly flammable) under ASHRAE Standard 34 [12], which introduces additional design and safety considerations when adapting or developing compressors for their use. For both R-290 and R-454C, these properties lead to several design implications such as an increase in displacement volume due to reduced volumetric capacity compared to R-410A, as illustrated in Fig. 1.

Table 1. Thermophysical properties of refrigerants under investigation [8-14]

Property	Units	R-410A	R-290	R-454C
Molecular Weight	$kg/kmol$	72.59	44.1	90.78
Liquid Density (at 25 °C)	kg/m^3	1059	492.1	1043
Vapor Density (at 25 °C)	kg/m^3	65.96	20.64	44.51
Latent Heat of Vaporization (at 25 °C)	kJ/kg	186.6	335.3	166.0
Ozone Depletion Potential (ODP)	–	0	0	0
Global Warming Potential (GWP) (100 yr)	–	2256	< 1	148
ASHRAE Classification	–	A1	A3	A2L

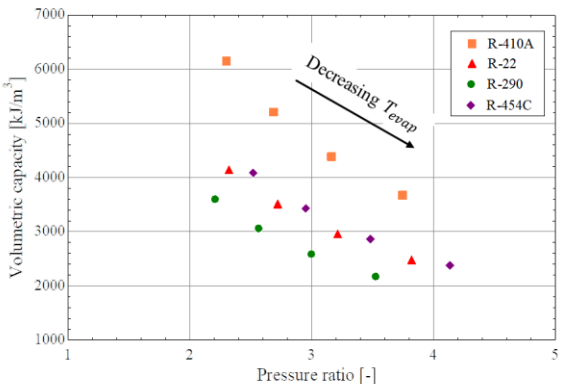

Figure 1. Comparison of volumetric capacity for R-410A, R-22, R-290 and R-454C for condensing temperature of 35 ºC and evaporating temperatures ranging from -10 ºC to 5 ºC in steps of 5 ºC, with superheat of 11 K and subcooling of 4 K.

These thermophysical disparities underscore the intricate link between refrigerant properties and compressor design. Scroll geometry parameters, such as built-in volume ratio, scroll wrap height, base radius, among others, strongly influence how efficiently the working fluid is compressed and how leakage, frictional, and thermal losses evolve. Multiple studies consistently demonstrate that although a simple drop-in approach can be convenient, it often leads to capacity-related issues and predictable and quantifiable performance penalties due to the inherent mismatch between the legacy compressor geometry and the thermodynamic behavior of the new fluid [15-16].

Recognizing these challenges highlights the necessity of refrigerant-specific compressor redesign and optimization [17]. To truly unlock the full potential of alternative fluids, compressor geometry must be tailored to the thermophysical properties of the new working fluid. This redesign process is resource-intensive and thus mandates the use of advanced, physics-based mechanistic models capable of performing extensive virtual soft optimization studies [18-19] before expensive physical prototypes are built, effectively accelerating the development of compliant, high-efficiency systems. While the availability of compressors using R-290 and R-454C on the market shows that such designs exist, a research gap exists to identify and quantify design intricacies necessary to achieve high compressor performance using these next-generation working fluids, as well as to explain their implications using high-fidelity, mechanistic models in the open literature.

The present work focuses on developing a deeper understanding of refrigerant–compressor interactions and how the fundamental thermophysical properties of R-290 and R-454C govern the holistic design of scroll compressors. Variations in gas density, latent heat, and thermal conductivity affect leakage characteristics, heat transfer mechanisms, and overall mechanical and thermodynamic losses, necessitating a reassessment of compressor architecture. To investigate these effects, this study combines experimental testing and high-fidelity modelling that evaluates scroll compressor operation with R-290 and R-454C. Experimental evaluations were conducted using a Hydrochlorofluorocarbon (HCFC)-based R-22 scroll compressor charged with R-290 and R-454C to establish performance trends and identify property-dependent deviations (Section 3.1). In parallel, compressors specifically designed for R-290 and R-410A were tested to quantify the performance achievable through refrigerant-specific design adaptation and develop a baseline for performance comparison, respectively (Section 3.1). Simultaneously, a comprehensive, physics-based mechanistic scroll compressor model has been developed and validated to serve as a high-accuracy predictive tool (Section 3.2). The overall objective is to leverage these insights and tools to define the necessary geometric modifications for next-generation compressors, systematically guiding the HVAC&R industry toward sustainable, high-performance refrigeration solutions mandated by global protocols.

2. Methodology

This section outlines the test stand utilized for the current study, provides an overview of the instruments and sensors used for data recording and presents the specifications of the scroll compressors under investigation. A hot-gas bypass stand, featuring R-22, R-290 and R-410A scroll compressors, is employed for this experimental study. Fig. 2 presents a schematic diagram illustrating the arrangement of various instruments. A legend for the schematic diagram, including the accuracy of the different instruments, is provided in Table 2.

In the hot-gas bypass test stand shown in Fig. 2, the compressed refrigerant exits the compressor and is throttled through the discharge valves (NV01, NV02 and MV01) for discharge pressure control before it is divided into two separate streams. One stream remains in a superheated vapor state and is throttled through hot-gas bypass valves (NV03, NV04 and MV02) back to suction pressure, which mainly controls the suction pressure. Finally, the remaining fraction of the split flow is condensed before being throttled through the liquid valves (MV03 and MV04) to suction pressure before being mixed with the throttled hot-gas flow to primarily control the compressor suction superheat.

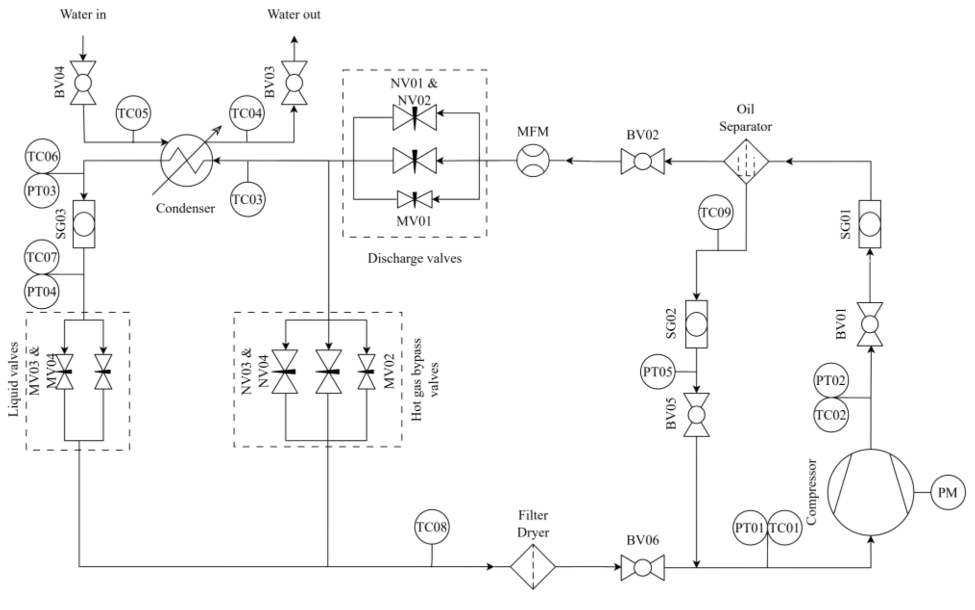

Figure 2. Schematic of the hot-gas bypass test stand utilized.

Measurement instruments used in this study inherently introduce systematic and random errors. Systematic errors were addressed by calibrating all sensors. The systematic error is estimated as Type B uncertainty, assuming a rectangular distribution for the sensor accuracy range [20]. The semi-range limit is denoted as a_i and the systematic standard uncertainty is calculated as shown in Eq. (1). Random errors that arise during data recording and were reduced by averaging data collected over a ten-minute steady-state period for each test condition [21]. Random error (Type A uncertainty) is evaluated statistically from repeated observations using Eq. (2), (3) and, (4). The combined uncertainty for each instrument or sensor is obtained by root-sum-of-squares (RSS) method as shown in Eq. (5).

$$u_s = \frac{a_i}{\sqrt{3}} \quad (1)$$

$$\bar{x} = \frac{1}{n}\sum_{i=1}^{n} x_i \quad (2)$$

$$s = \sqrt{\frac{1}{n-1}\sum_{i=1}^{n}(x_i - \bar{x})^2} \quad (3)$$

$$u_r = \frac{s}{\sqrt{n}} \quad (4)$$

$$u_c(\bar{x}) = \sqrt{u_s{}^2 + u_r^2} \quad (5)$$

Table 2. Nomenclature and specifications of components of hot-gas bypass test stand.

Symbol	Name	Manufacturer/ Model	Range	Accuracy (± half-width a_i)
PT01, 03, 04 & 05	Pressure Transducer	Honeywell/ PX2AF1XX500PAAAX	0 to 500 psi	± 0.25 %[1]
PT02	Pressure Transducer	Setra/ 206110CPG2M22028NN	0 to 1,000 psi	± 0.13 %[1]
TC01, 02 & 09	Thermocouple	Omega/ Type T/ TMQSS-062(E)-6	> 0 °C to 350 °C	± 1 °C or 0.75 %[2]
			-200 °C to 0 °C	± 1 °C or 1.5 %[2]
TC03 to 08	Thermocouple	Omega/ Type T/ TMQSS-125(E)-6	> 0 °C to 350 °C	± 1 °C or 0.75 %[2]
			-200 °C to 0 °C	± 1 °C or 1.5 %[2]
MFM	Mass Flow Meter	Micromotion/ CMF050M314NU	0 to 6,800 kg/h	± 0.35 %[3]
PM	Power Meter	Ohio Semitronics/ GW5-059EG	0 to 20kW	± 0.2 %[3]
SG01 to 03	Sight Glass	-	-	-
BV01 to 06	Ball Valve	-	-	-
NV01 to 04	Needle Valve	-	-	-
MV01 to 04	Meter Valve	-	-	-

The derived quantities $y = f(\bar{x}_1, \bar{x}_2 \cdots, \bar{x}_N)$ obtained using the mean estimates for the input quantities given by $\bar{x}_j$ as calculated in Eq. (2). The uncertainty propagation calculation for the derived quantities is performed using EES software [10]. The combined uncertainty for the estimate y of the measurand, or quantity being measured, Y is calculated as shown in Eq. (6).

$$u_c(y) = \sqrt{\sum_{j=1}^{N}\left(\frac{\partial f}{\partial \bar{x}_j}\right)^2 u_c^2(\bar{x}_j)} \quad (6)$$

3. Results and Discussion

This section presents the experimental evaluation and subsequent model validation aimed at understanding how refrigerant properties influence compressor design and performance. The discussion begins with the comparative testing of three fixed-speed scroll compressors under a range of operating conditions (Section 3.1). Particular attention is given to the behavior of R-290, both as drop-in fluid in an HCFC compressor and in a dedicated R-290 compressor, to assess how refrigerant-specific design adaptation affects mass flow rate, power consumption and efficiency. The recorded data demonstrates that for the next generation refrigerants,

[1] Of Full-Scale Span
[2] Whichever value is greater.
[3] Of Measured Value

R-290 and R-454C, achieving comparable capacity and efficiency to R-410A requires careful geometric redesign rather than simple displacement scaling. Building on these experimental findings, the section also provides an overview of the high-fidelity mechanistic scroll compressor model that is developed, calibrated and validated using the experimental data from the baseline R-410A compressor (Section 3.2). The mechanistic model captures thermodynamic, mechanical, and thermal effects, providing a robust platform for future soft optimization studies aimed at maximizing the performance for alternative refrigerants.

3.1. Scroll Compressors Testing and Performance Comparison

In this section, three fixed-speed scroll compressors were evaluated: an R-22 compressor (model ZR32K5E-PFJ), an R-290 compressor (model ZH11KCU-PFV), and an R-410A compressor (model ZP31K6E-PFV), with displacement volumes of 44.08 cm³/rev, 82.59 cm³/rev, and 29.33 cm³/rev, respectively, as reported by the manufacturer. The R-22 compressor was used for drop-in testing with R-290 and R-454C to examine performance trends and assess design implications, since R-22 has a volumetric capacity closer to these drop-in fluids than R-410A (as shown in Fig. 1), allowing for more stable test stand operation. The R-290 compressor was evaluated with R-290 refrigerant to characterize its design-specific performance. The R-410A compressor served as a baseline unit for developing and validating a detailed mechanistic model.

The tested operating conditions, measured parameters, and corresponding uncertainties are summarized in Table A1 to Table A4 (Appendix A), encompassing evaporating temperatures from −10 °C to 5 °C and condensing temperatures of 35 °C and 45 °C. The overall isentropic efficiency, volumetric efficiency, cooling capacity and volumetric capacity are calculated using Eq. (7) to (10), respectively. Performance trends obtained from the experiments for the normalized data calculated using Eq. (11) are presented in Fig. 3.

$$\eta_{oi} = \frac{\dot{m}\left(h_{dis,s} - h_{suc}\right)}{\dot{W}_{elec}} \tag{7}$$

$$\eta_v = \frac{\dot{m}}{\rho_{suc} V_{disp} N} \tag{8}$$

$$\dot{Q}_{evap} = \dot{m}\left(h_{suc} - h_{evap,in}\right) \tag{9}$$

$$Q_{vol} = \rho_{suc}\left(h_{suc} - h_{evap,in}\right) = \frac{\dot{Q}_{evap}}{\eta_v V_{disp} N} \tag{10}$$

$$X_{norm} = \frac{X}{X_{ref}} \tag{11}$$

where X represents data for mass flow rate, power consumption, overall isentropic efficiency, volumetric efficiency, cooling capacity, volumetric capacity and X_{ref} corresponds to the maximum observed value of each respective parameter across the refrigerants evaluated.

The influence of refrigerant thermophysical properties is evident in the observed performance trends across varying pressure ratios (achieved by decreasing the evaporating temperature, T_{evap}, from 5 °C to −10 °C). As shown in Fig. 3 (a), a reduction in T_{evap} increases the pressure ratio and decreases the inlet density, leading to a lower mass flow rate for all refrigerants. The relative magnitude of the mass flow rate among refrigerants is governed by the combined effect of inlet density and compressor displacement volume.

In the drop-in tests using the R-22 compressor, R-454C exhibits higher inlet density and therefore has higher mass flow rate compared to R-290. Although R-410A possesses a higher inlet density than R-454C, the smaller displacement volume of R-410A compressor (29.33 cm³/rev) results in a lower mass flow rate. For the R-290-specific compressor, despite its lowest inlet density, the larger displacement (82.59 cm³/rev) enables a mass flow rate comparable to R-410A under certain conditions.

The higher mass flow rate of R-454C in the drop-in configuration is accompanied by higher power consumption, as shown in Fig. 3 (b). This can be attributed to its higher operating pressure ratio compared to the other refrigerants. Conversely, R-290 (drop-in) exhibits the lowest power consumption due to its lower mass flow rate. Interestingly, the R-290 commercially available compressor shows the highest absolute power consumption among all units, primarily due to its larger physical size that results in greater losses from larger bearings and motor components. Additionally, the use of PAG oil in the R-290 commercially available compressor, which differs from the POE oil used in the drop-in study with the R-22 compressor and also for testing of the R-410A compressor, introduces differences in refrigerant-oil solubility and viscosity characteristics, potentially influencing both mechanical and thermal losses.

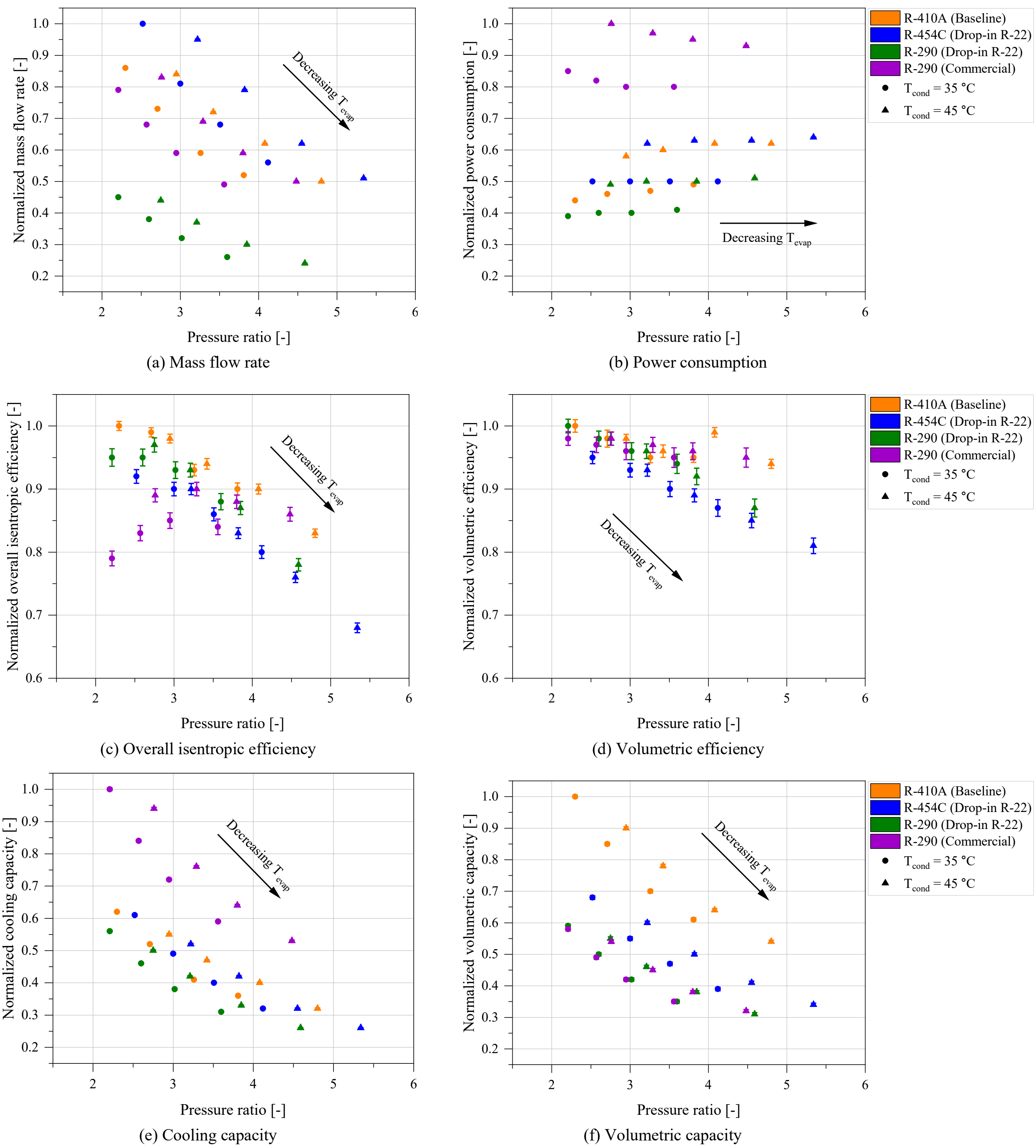

Figure 3. Trends of normalized data for tested compressors with refrigerants R-410A, R-290, and R-454C across the operating conditions defined in Appendix A. (Error bands for certain parameters are negligible due to relatively low measurement uncertainty. Refer to Appendix A for experimental and uncertainty data.)

Another notable observation is that, for the testing with R-22 and R-410A compressors, power consumption remains nearly constant with increasing pressure ratio at a fixed condensing temperature. However, for the R-290 compressor, power consumption decreases with pressure ratio at a fixed condensing temperature. This contrasting behaviour arises from the balance between reduced inlet density (resulting in reduced mass flow rate) and increasing pressure ratio as T_{evap} decreases. In the drop-in tests with R-290 and R-454C, as well as for the R-410A compressor, these two effects largely balance each other out. In contrast, for the R-290 compressor, the reduction in mass flow rate is more dominant, leading to a net decrease in power consumption as the pressure ratio increases. These findings underscore the importance of detailed compressor modelling to capture and interpret such phenomena, enabling optimization of geometry and loss mechanisms for each refrigerant. A mechanistic scroll compressor model, developed and validated using R-410A test data, is introduced in Section 3.2.

As depicted in Fig. 3 (c) and (d), both overall isentropic and volumetric efficiencies decrease with increasing pressure ratio for all refrigerants. For the drop-in tests, R-290 demonstrates higher overall isentropic and volumetric efficiency due to its lower operating pressure ratio and reduced discharge temperatures, which minimize leakage and mechanical losses. These results highlight the potential of R-290 as a high-efficiency replacement when system design is optimized. R-454C, on the other hand, operates at higher pressure ratios and does not reach a distinct overall isentropic efficiency peak within the reported testing range, indicating that further increase in evaporating temperatures may lead to over-compression losses and reduced efficiency. The R-410A baseline compressor achieves the highest overall isentropic efficiency, while the commercially available R-290 compressor exhibits the lowest, suggesting opportunities for improving commercial hydrocarbon (HC) compressor designs through geometric and mechanical refinements.

Cooling and volumetric capacities, presented in Fig. 3 (e) and (f), respectively, were calculated assuming a condenser outlet subcooling of 4 K to determine the evaporator inlet condition. Despite the high latent heat of vaporization of R-290, its low inlet density limits cooling capacity for a given displacement in case of drop-in evaluation. The higher density of R-454C enables greater cooling capacity than R-290 (drop-in), though still below that of R-410A, due to the lower latent heat of R-454C. R-410A achieves higher cooling capacity than both drop-in fluids due to its high density, while the R-290 commercially-available unit, with its larger displacement, delivers the highest cooling capacity. These results clearly indicate that matching the capacity of current HFC compressors with the alternatives requires increased displacement volume, owing to their inherently lower volumetric capacities (Fig. 3 (f)).

The trends in Fig. 3 emphasize the inherent limitations of a drop-in replacement strategy. Achieving comparable performance with alternative refrigerants necessitates a comprehensive compressor redesign that considers not only displacement volume, but also leakage control, heat transfer, frictional and mechanical losses, and motor characteristics. Simply scaling the displacement volume is insufficient, as this can be accomplished through multiple geometric modifications in a scroll compressor, such as increasing scroll height, extending the involute length, or reducing scroll thickness, each of which influences internal flow behaviour and losses differently. Furthermore, minimizing mechanical and thermal losses requires identifying and quantifying the contributions of individual components, including bearings, scrolls, and the motor, and understanding how these losses are distributed throughout the compressor. Experimental evaluation alone cannot resolve these complex interacting mechanisms or reveal the optimal configuration for minimizing losses. Therefore, detailed mechanistic modelling is essential to isolate and reduce specific loss mechanisms. The experimental insights presented here form the foundation for developing such a model, described in Section 3.2, which aims to guide the design of next-generation compressors optimized for alternative refrigerants.

3.2. Model Description and Validation

As discussed in Section 3.1, it is difficult to isolate design modifications for compressors from experiments alone. To address this limitation of experiments and better understand how geometry and working fluid properties influence the compressor performance, a physics-based mechanistic scroll compressor model was developed in the Positive Displacement Simulation (PDSim) framework [22-23]. PDSim enables high-fidelity modeling of positive displacement machines by defining geometry, flow paths, leakage mechanisms, and thermal and mechanical losses in a modular environment to capture the coupled thermodynamic, mechanical, and thermal processes governing compressor operation. The geometric sub-model defines key compressor parameters such as displacement volume, volume ratio, scroll wrap height, and other parameters, to determine the instantaneous working volumes and their evolution during compression. The refrigerant properties during the compression process are evaluated using REFPROP [9] and CoolProp [11] to ensure accurate real-fluid representation.

The working domain was discretized into control volumes connected by flow paths representing suction, discharge, and internal leakages. Radial and flank leakages, which depend on the manufacturing clearances and pressure-induced deformation, were represented using empirical correlations that relate effective leakage gaps to pressure ratio [24]. The electric motor driving the compressor was modeled using a torque-slip based efficiency map to account for motor losses. For soft optimization studies involving multiple refrigerants and geometries, a pressure-ratio based motor efficiency correlation was developed to eliminate dependence on a specific compressor design and refrigerant. Mechanical frictional losses arising from journal and thrust bearings were computed from radial and axial forces acting on the orbiting scroll.

To accurately predict the refrigerant discharge temperature, a multi-lump thermal model representing key heat transfer paths between the scrolls, shell, motor, and gas regions [25-26] was implemented. The heat interactions between the lumped masses were captured using conductive and convective thermal resistances. Transient mass and energy conservation equations were solved iteratively for each control volume, while the overall periodic steady state solution was obtained using a nonlinear solver coupled with an adaptive Runge-Kutta integration scheme [27].

The assumptions used for analysis of the control volumes include, uniform temperature and pressure, negligible kinetic energy and gravitational effects, thermal interactions occur through heat transfer, and mass flow is accounted by evaluating flow paths connected to the control volumes. The conservation of mass and energy for the control volumes is defined using Eq. (12) and (13), respectively as discussed in [22].

$$\frac{dm}{d\theta} = \frac{1}{\omega}\sum_i \dot{m}_i \tag{12}$$

$$\frac{dU}{dt} = \dot{Q} + \dot{W} + \sum_i \dot{m}_i\, h_i \tag{13}$$

where $\dot{m}_i$ represents mass flow rate for the i-th flow path (positive if flow is entering the control volume), ω is compressor rotational speed, $\dot{Q}$ represents heat entering the control volume, $\dot{W}$ is boundary work, and U is total internal energy [22-23].

Experimental data for model calibration were obtained from tests performed on an R-410A scroll compressor (model ZP31K6E-PFV). The measured data and corresponding operating conditions are summarized in Table A4 (Appendix A). The iterative steps involved in the calibration procedure are illustrated in Fig. 4.

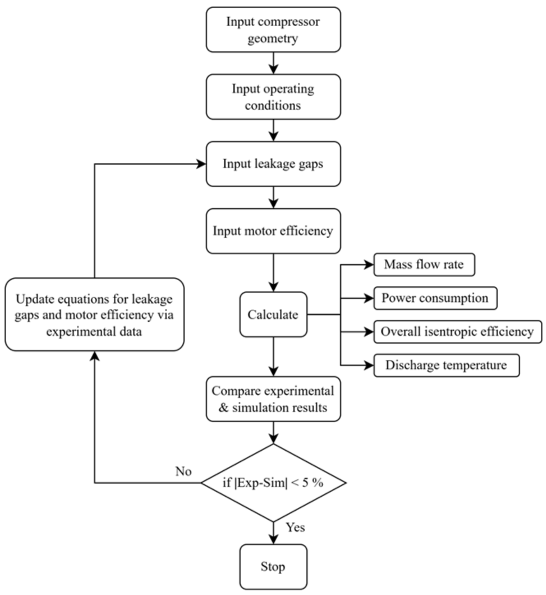

Figure 4. Flowchart representing the steps involved in model calibration.

Using the measured geometry of the modeled compressor, the accuracy of model in predicting key performance indicators, namely mass flow rate, power consumption, overall isentropic efficiency, and discharge temperature, is iteratively improved. This process involves the calibration of correlations for leakage gaps, the development of a motor efficiency map using the collected experimental data and transitioning from a simpler single-lump framework to a more complex multi-lump architecture to capture thermal interaction between the lumps. The goal of this calibration is to achieve a predictive accuracy within a ± 5 % (and ± 5 ºC) error margin.

The validation of the calibrated model is as presented in Fig. 5. The mean absolute percentage errors (MAPE) were 2.4 %, 1.18 % and 2.12 % for mass flow rate, power consumption, and overall isentropic efficiency, respectively, with a mean absolute error (MAE) of 1.74 °C for discharge temperature. These results confirm the strong predictive capability of model and establish a reliable foundation for subsequent soft optimization studies and refrigerant-specific redesign, aimed at enhancing compressor performance for alternative refrigerants.

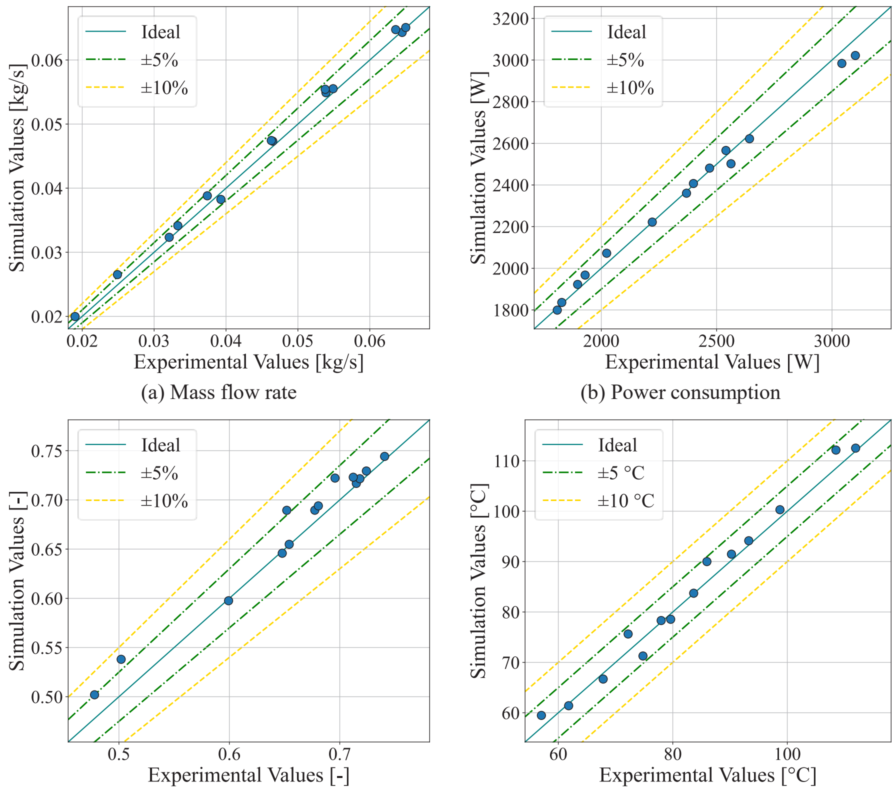

(a) Mass flow rate (b) Power consumption

(c) Overall isentropic efficiency (d) Discharge temperature

Figure 5. Mechanistic model validation with experimental data obtained for R-410A scroll compressor (model ZP31K6E-PFV) for operating conditions mentioned in Table A4 (refer Appendix A).

4. Conclusion

The transition to alternative refrigerants in vapor compression systems highlights the critical influence of thermophysical properties on compressor performance. This study successfully combines experimental testing with mechanistic modelling to evaluate next-generation refrigerants, R-290 and R-454C, in scroll compressors as a replacement for R-410A. The results underscore the necessity for refrigerant-specific compressor redesign to improve compressor performance and establish key takeaways supporting this conclusion.

- Property-driven performance shifts**:** The unique thermophysical properties of R-290 (low vapor density and high latent heat) and R-454C (moderate density with reduced latent heat) lead to significant differences in compressor performance parameters like volumetric capacity, discharge temperature, and efficiency compared to R-410A.
- Limitation of experimental study: Experimental data alone is insufficient to identify the optimal geometric changes (e.g. scroll height, built-in volume ratio) needed to improve compressor performance for new refrigerants.
- Validated modelling is essential for optimization: A mechanistic scroll compressor model, validated against experimental data (achieving a MAPE of 1.18% and 2.4 % for power consumption and mass flow rate, respectively), provides a reliable tool for geometry optimization.

Future work will focus on the application of the validated mechanistic model for performing parametric studies aimed at maximizing the performance of scroll compressors for alternative refrigerants, using the developed soft optimization methodology. This effort will define the necessary geometry modifications for an optimal transition to sustainable refrigerants.

5. Nomenclature

a_i	Half-width of the interval or Semi range limit	$\dot{Q}_{evap}$	Cooling capacity
ρ_{suc}	Compressor inlet density	Q_{vol}	Volumetric capacity
η_{oi}	Overall isentropic efficiency	s	Standard deviation
η_v	Volumetric efficiency	u_c	Combined uncertainty

h_{suc}	Specific enthalpy at compressor inlet	u_r	Random standard uncertainty
$h_{dis,s}$	Isentropic compression outlet specific enthalpy	u_s	Systematic standard uncertainty
$h_{evap,in}$	Evaporator inlet specific enthalpy	V_{disp}	Compressor displacement volume
$\dot{m}$	Mass flow rate	$\dot{W}_{elec}$	Electrical power consumption
n	Number of readings	x_i	Value of i^{th} recorded parameter
N	Compressor speed	$\bar{x}$	Arithmetic mean

Funding Declaration

This manuscript has been authored by UT-Battelle, LLC, under contract DE-AC05-00OR22725 with the US Department of Energy (DOE). The US government retains and the publisher, by accepting the article for publication, acknowledges that the US government retains a nonexclusive, irrevocable, worldwide license to publish or reproduce the published form of this manuscript, or allow others to do so, for US government purposes. DOE will provide public access to these results of federally sponsored research in accordance with the DOE Public Access Plan (http://energy.gov/downloads/doe-public-access-plan).

References

[1] United Nations Environment Programme (UNEP). *Montreal Protocol on Substances that Deplete the Ozone Layer.* Montreal: UNEP; 1987.
[2] United Nations Environment Programme (UNEP). *Kigali Amendment to the Montreal Protocol on Substances that Deplete the Ozone Layer.* Kigali: UNEP; 2016.
[3] Kumma, N., & Kruthiventi, S. H. (2023). Current status of refrigerants used in domestic applications: A review. *Renewable and Sustainable Energy Reviews*, *189*, 114073.
[4] European Union. *Regulation (EU) No 517/2014 of the European Parliament and of the Council on fluorinated greenhouse gases and repealing Regulation (EC) No 842/2006.* Brussels: Official Journal of the European Union; 2014.Strunk Jr W, White EB. *The elements of style*. 3rd ed. New York: Macmillan; 1979.
[5] United States. American Innovation and Manufacturing (AIM) Act of 2020. Washington, D.C.: U.S. Congress; 2020.
[6] Issa, A. a. B., Liang, C., Liu, H., Groll, E. A., & Ziviani, D. (2025). Experimental analysis of a liquid-to-liquid two-stage R290 heat pump system for residential cold-climate applications. *Applied Thermal Engineering*, *127223*.
[7] Llopis, R., Calleja-Anta, D., Sánchez, D., Nebot-Andrés, L., Catalán-Gil, J., & Cabello, R. (2019). R-454C, R-459B, R-457A and R-455A as low-GWP replacements of R-404A: Experimental evaluation and optimization. *International Journal of Refrigeration*, *106*, 133-143.
[8] Intergovernmental Panel on Climate Change (IPCC). *Climate Change 2021: The Physical Science Basis. Contribution of Working Group I to the Sixth Assessment Report of the Intergovernmental Panel on Climate Change.* Cambridge: Cambridge University Press; 2021.
[9] Lemmon, E. W., Huber, M. L., & McLinden, M. O. (2018). *NIST Reference Fluid Thermodynamic and Transport Properties Database (REFPROP), Version 10.0.* National Institute of Standards and Technology, Gaithersburg, MD, USA. https://doi.org/10.18434/T4JS3C
[10] Klein, S. A., & Alvarado, F. L. (2019). *Engineering Equation Solver (EES), Version 10.388.* F-Chart Software, Madison, WI, USA. Available at: https://fchartsoftware.com
[11] Bell, I. H., Wronski, J., Quoilin, S., & Lemort, V. (2014). *Pure and pseudo-pure fluid thermophysical property evaluation and the open-source thermophysical property library CoolProp.* Industrial & Engineering Chemistry Research, 53(6), 2498–2508. https://doi.org/10.1021/ie4033999
[12] ASHRAE. (2019). *ANSI/ASHRAE Standard 34-2019: Designation and Safety Classification of Refrigerants.* American Society of Heating, Refrigerating and Air-Conditioning Engineers, Inc., Atlanta, GA, USA.
[13] ASHRAE. (1997). *ASHRAE Handbook—Fundamentals.* American Society of Heating, Refrigerating and Air-Conditioning Engineers, Inc., Atlanta, GA, USA.
[14] World Meteorological Organization (WMO). (2014). *Scientific Assessment of Ozone Depletion: 2014.* Global Ozone Research and Monitoring Project—Report No. 55, Geneva, Switzerland.

[15] Braga, C. H., Martins, L. V., Pabon, J. J., Machado, L., & Duarte, W. M. (2025). Energetic, economic and environmental (3E) analysis of R290, R454C and R465A for drop-in split type air conditioning running on R22. *Case Studies in Thermal Engineering*, *69*, 105988.

[16] Ibrahim, O. a. A., Kadhim, S. A., Hammoodi, K. A., Rashid, F. L., & Askar, A. H. (2024). Review of hydrocarbon refrigerants as drop-in alternatives to high-GWP refrigerants in VCR systems: The case of R290. *Cleaner Engineering and Technology*, *100825*.

[17] Tanveer, M. M., Bradshaw, C. R., Orosz, J., & Kemp, G. (2024). Pseudo-optimum geometries for 1–100 ton spool compressors with low-GWP refrigerants. *International Journal of Refrigeration, 157*, 12–22. https://doi.org/10.1016/j.ijrefrig.2023.10.005

[18] Alabdulkarem, A., Eldeeb, R., Hwang, Y., Aute, V., & Radermacher, R. (2015). Testing, simulation and soft-optimization of R410A low-GWP alternatives in heat pump system. *International Journal of Refrigeration*, *60*, 106-117.

[19] Guth, T., & Atakan, B. (2021). Semi-empirical model of a variable speed scroll compressor for R-290 with the focus on compressor efficiencies and transferability. *International Journal of Refrigeration, 128,* 93–107. https://doi.org/10.1016/j.ijrefrig.2021.04.013

[20] United Kingdom Accreditation Service (UKAS). (2024). *M3003: The Expression of Uncertainty and Confidence in Measurement.* Edition 6, March 2024. United Kingdom Accreditation Service, Staines-upon-Thames, United Kingdom. Available at: https://www.ukas.com

[21] American Society of Mechanical Engineers (ASME). (2022). *ASME PTC 10-2022: Axial and Centrifugal Compressors Performance Test Codes.* American Society of Mechanical Engineers, New York, NY, USA.

[22] Bell, I. H., Ziviani, D., Lemort, V., Bradshaw, C. R., Mathison, M., Horton, W. T., Braun, J. E., & Groll, E. A. (2020). *PDSim: A general quasi-steady modeling approach for positive displacement compressors and expanders. International Journal of Refrigeration*, 110, Article 323–339. https://doi.org/10.1016/j.ijrefrig.2019.09.002

[23] Ziviani, D., Bell, I. H., Zhang, X., Lemort, V., De Paepe, M., Braun, J. E., & Groll, E. A. (2020). *PDSim: Demonstrating the capabilities of an open-source simulation framework for positive displacement compressors and expanders. International Journal of Refrigeration*, 110, 323–339. https://doi.org/10.1016/j.ijrefrig.2019.10.015

[24] Chen, Y., Halm, N. P., Groll, E. A., & Braun, J. E. (2002). Mathematical modeling of scroll compressors—Part I: Compression process modeling. *International Journal of Refrigeration*, 25(6), 731–750. https://doi.org/10.1016/S0140-7007(01)00071-8

[25] Pereira, E. L. L., & Deschamps, C. J. (2010). A Lumped Thermodynamic Model for Scroll Compressors with Special Attention to the Geometric Characterization during the Discharge Process. *International Compressor Engineering Conference*. Paper 2007.

[26] Diniz, M. C., Pereira, E. L. L., & Deschamps, C. J. (2014). A lumped-parameter thermal model for scroll compressors including the solution for the temperature distribution along the scroll wraps. *International Journal of Refrigeration*, *53*, 184-194. https://doi.org/10.1016/j.ijrefrig.2014.01.003

[27] Kreyszig, E. (2006). *Advanced Engineering Mathematics* (9th ed.). John Wiley and Sons.

Appendix A

The operating conditions recorded for the experimental drop-in testing of R-290 and R-454C using R-22 scroll compressor, are summarized in Table A1, and Table A2, respectively. The recorded operating conditions for testing of R-290 and R-410A scroll compressors are presented in Table A3, and Table A4, respectively. Each table also includes the uncertainties associated with the recorded and calculated parameters.

Table A1 Recorded operating conditions and associated uncertainties for R-290 drop-in testing in R-22 scroll (ZR32K5E-PFJ)

Point #	T_{evap}	T_{cond}	ΔT_{sup}	T_{disc}	$\dot{m}$	$\dot{W}_{elec}$	η_{oi}	η_v	$\dot{Q}_{evap}$	Q_{vol}	$u_{T_{disc}}$	$u_{\dot{m}}$	$u_{\dot{W}_{elec}}$	$u_{\eta_{oi}}$	u_{η_v}	$u_{\dot{Q}_{evap}}$	$u_{Q_{vol}}$
	ºC	ºC	ºC	ºC	g/s	W	-	-	W	kJ/m^3	ºC	%	%	-	-	W	kJ/m^3
1	-10.5	35.3	11.4	65.0	16.7	1668	0.6378	0.9122	4998	2131	0.58	0.2	0.12	9.25E-03	1.49E-02	21.21	32.72
2	-5.2	35.0	11.2	59.9	20.18	1648	0.6724	0.9376	6178	2563	0.58	0.2	0.12	9.55E-03	1.32E-02	26.12	33.5
3	0.3	35.9	11.0	57.2	24.25	1665	0.6895	0.9551	7515	3060	0.58	0.2	0.12	9.62E-03	1.16E-02	31.9	34.06
4	5.2	35.2	10.7	54.6	28.54	1624	0.6876	0.9746	9057	3614	0.58	0.2	0.12	1.00E-02	1.05E-02	38.33	35.13
5	-10.5	45.7	11.2	82.9	15.5	2091	0.5622	0.847	4172	1916	0.58	0.2	0.12	7.13E-03	1.38E-02	18.9	29.34

6	-5.3	45.4	11.5	74.8	19.26	2064	0.6272	0.8987	5332	2307	0.58	0.2	0.12	7.60E-03	1.27E-02	23.96	30.13
7	0.7	45.6	11.1	69.5	23.91	2060	0.6726	0.9311	6759	2823	0.58	0.2	0.12	7.86E-03	1.12E-02	30.39	30.92
8	5.7	45.5	10.5	65.4	28.33	2015	0.7033	0.9515	8164	3337	0.58	0.2	0.12	8.18E-03	1.01E-02	36.74	31.81

Table A2 Recorded operating conditions and associated uncertainties for R-454C drop-in testing in R-22 scroll (ZR32K5E-PFJ)

Point #	T_{evap} ºC	T_{cond} ºC	ΔT_{sup} ºC	T_{disc} ºC	$\dot{m}$ g/s	$\dot{W}_{elec}$ W	η_{oi} -	η_v -	$\dot{Q}_{evap}$ W	Q_{vol} kJ/m^3	$u_{T_{disc}}$ ºC	$u_{\dot{m}}$ %	$u_{\dot{W}_{elec}}$ %	$u_{\eta_{oi}}$ -	u_{η_v} -	$u_{\dot{Q}_{evap}}$ W	$u_{Q_{vol}}$ kJ/m^3
1	-9.7	35.3	11.9	73.2	35.67	2066	0.5783	0.8523	5264	2402	0.58	0.2	0.12	7.24E-03	1.29E-02	23.42	33.68
2	-4.8	35.6	10.7	67.1	43.61	2070	0.6215	0.8815	6496	2866	0.58	0.2	0.12	7.48E-03	1.16E-02	29.09	34.36
3	-0.3	35.2	11.7	63.5	51.57	2042	0.6525	0.9058	7901	3392	0.58	0.2	0.12	7.74E-03	1.05E-02	35.09	35.36
4	5.6	35.7	10.1	58.7	63.89	2066	0.6648	0.9278	9854	4130	0.58	0.2	0.12	7.87E-03	9.40E-03	44.37	36.4
5	-10.0	45.9	12.0	94.8	32.44	2633	0.4894	0.7853	4231	2095	0.58	0.2	0.12	5.51E-03	1.20E-02	20.53	29.59
6	-5.8	45.3	11.8	85.4	39.52	2574	0.5492	0.8285	5286	2482	0.58	0.2	0.12	5.93E-03	1.12E-02	25.47	30.49
7	0.0	46.0	10.9	77.6	50.27	2610	0.6039	0.8714	6800	3035	0.58	0.2	0.12	6.19E-03	1.01E-02	33.06	31.22
8	5.0	45.4	11.0	72.0	60.95	2559	0.6498	0.905	8476	3642	0.58	0.2	0.12	6.54E-03	9.26E-03	40.99	32.42

Table A3 Recorded operating conditions and associated uncertainties for R-290 scroll compressor (ZH11KCU-PFV)

Point #	T_{evap} ºC	T_{cond} ºC	ΔT_{sup} ºC	T_{disc} ºC	$\dot{m}$ g/s	$\dot{W}_{elec}$ W	η_{oi} -	η_v -	$\dot{Q}_{evap}$ W	Q_{vol} kJ/m^3	$u_{T_{disc}}$ ºC	$u_{\dot{m}}$ %	$u_{\dot{W}_{elec}}$ %	$u_{\eta_{oi}}$ -	u_{η_v} -	$u_{\dot{Q}_{evap}}$ W	$u_{Q_{vol}}$ kJ/m^3
1	-10.6	34.6	11.8	65.2	31.61	3274	0.6104	0.9267	9535	2136	0.58	0.2	0.12	8.94E-03	1.51E-02	40.26	32.92
2	-5.3	34.0	11.0	60.8	37.79	3302	0.614	0.9366	11654	2583	0.58	0.2	0.12	8.90E-03	1.32E-02	49.08	33.83
3	-1.0	33.8	10.5	58.6	43.45	3366	0.6009	0.9448	13625	2993	0.58	0.2	0.12	8.77E-03	1.19E-02	57.35	34.56
4	4.2	34.0	11.7	59.0	50.71	3484	0.5735	0.9549	16281	3539	0.58	0.2	0.12	8.55E-03	1.05E-02	68.21	35.32
5	-10.1	45.2	11.9	75.6	31.9	3828	0.6243	0.9228	8689	1954	0.58	0.2	0.12	7.92E-03	1.49E-02	39.05	29.58
6	-5.2	45.0	11.5	72.4	37.59	3914	0.6388	0.9313	10455	2330	0.58	0.2	0.12	7.77E-03	1.31E-02	46.86	30.27
7	-0.3	45.3	11.2	69.8	43.91	3996	0.6498	0.9405	12418	2741	0.58	0.2	0.12	7.66E-03	1.16E-02	55.67	30.89
8	5.7	45.4	10.9	67.4	52.83	4112	0.6453	0.9513	15262	3330	0.58	0.2	0.12	7.50E-03	1.02E-02	68.51	31.81

Table A4 Recorded operating conditions and associated uncertainties for R-410A scroll compressor (ZP31K6E-PFV)

Point #	T_{evap} ºC	T_{cond} ºC	ΔT_{sup} ºC	T_{disc} ºC	$\dot{m}$ g/s	$\dot{W}_{elec}$ W	η_{oi} -	η_v -	$\dot{Q}_{evap}$ W	Q_{vol} kJ/m^3	$u_{T_{disc}}$ ºC	$u_{\dot{m}}$ %	$u_{\dot{W}_{elec}}$ %	$u_{\eta_{oi}}$ -	u_{η_v} -	$u_{\dot{Q}_{evap}}$ W	$u_{Q_{vol}}$ kJ/m^3
1	9.3	34.7	11.0	57.1	64.51	1809	0.7136	0.9953	12069	7087	0.58	0.2	0.12	5.39E-03	9.09E-03	27.17	30.68
2	4.7	34.6	10.6	61.8	54.87	1829	0.7235	0.9722	10171	6115	0.58	0.2	0.12	5.16E-03	9.68E-03	21.76	30.03
3	10.4	45.5	12.0	72.2	65.00	2369	0.7398	0.9768	11002	6583	0.58	0.2	0.12	4.57E-03	1.03E-02	16.53	29.46
4	0.0	35.4	11.2	67.8	46.54	1898	0.7186	0.9572	8498	5189	0.58	0.2	0.12	5.21E-03	1.32E-02	12.62	31.66
5	4.9	45.2	10.9	78.0	53.85	2399	0.7121	0.9504	8986	5526	0.58	0.2	0.12	5.09E-03	6.71E-03	46.6	28.89
6	10.5	55.1	11.0	86.0	63.59	3043	0.6954	0.9467	9516	5875	0.58	0.2	0.12	6.38E-03	8.87E-03	26.73	34.3
7	-5.8	35.2	10.4	74.8	37.40	1930	0.6763	0.9236	6731	4259	0.58	0.2	0.12	6.67E-03	8.04E-03	34.06	35.05
8	0.7	45.7	11.2	83.7	46.32	2469	0.6817	0.9352	7617	4760	0.58	0.2	0.12	6.16E-03	9.66E-03	23.34	33.32
9	5.7	54.8	10.9	93.3	53.84	3101	0.6527	0.9256	7989	5044	0.58	0.2	0.12	5.50E-03	7.75E-03	32.99	31.21
10	-9.3	36.7	10.3	79.6	33.30	2023	0.6544	0.9231	5854	3706	0.58	0.2	0.12	6.96E-03	7.53E-03	41.24	36.22
11	-5.4	45.0	12.1	90.2	39.29	2562	0.6488	0.9674	6457	3901	0.58	0.2	0.12	5.75E-03	7.31E-03	39.28	32.05
12	-9.9	45.4	11.8	98.7	32.11	2540	0.5997	0.9158	5179	3305	0.58	0.2	0.12	4.80E-03	7.02E-03	38.45	28.29
13	-15.0	45.5	11.0	111.9	24.90	2642	0.501	0.8422	3937	2732	0.58	0.2	0.12	7.13E-03	7.17E-03	49.56	37.08
14	-22.7	37.6	9.4	108.5	19.00	2221	0.4775	0.8401	3178	2211	0.58	0.2	0.12	5.98E-03	6.89E-03	48.58	32.82